Investigation on the effect of electrode tip on formation of metal droplets and temperature profile in a vibrating electrode electroslag remelting process

Wang, Fang; Baleta, Jakov; Wang, Qiang; Li, Baokuan

Research Article

Fang Wang*, Jakov Baleta, Qiang Wang, and Baokuan Li

Investigation on the effect of electrode tip on formation of metal droplets and temperature profile in a vibrating electrode electroslag remelting process

https://doi.org/10.1515/phys-2019-0078
Received Aug 12, 2019; accepted Sep 20, 2019

Abstract: In the present work, a transient full-coupled modelling approach has been put forward to study the effect of electrode tip on formation of metal droplets and temperature profile in the electromagnetically-controlled electroslag-remelting furnace with vibrating electrode. The electromagnetic field, momentum and energy conservation equations are solved simultaneously based on the finite volume method. The interface of slag and metal is traced using the volume of fluid approach. The results show that in the case of cone tip electrode the average dimension of metal droplets is smaller compared to the flat tip electrode. In addition, the bigger and stretched metal droplets are not observed with the cone tip electrode. The temperature fields with the cone tip electrode are distributed in a prominent periodic pattern compared to the case with flat tip electrode. The maximum temperature zone with the cone tip electrode is located along the z axial in the upper part of slag, not in the lower part. When the frequency changes from 0.17 Hz to 1 Hz, the maximum temperature reduces from 2050 K to 1985 K and the peak value of velocity decreases from 0.20 m/s to 0.125 m/s. When the vibration amplitude varies from 3mm to 6mm, the maximum temperature in the slag cover drops by 3.9% and the peak value of velocity rises by 16.7%.

Keywords: vibrating electrode electroslag remelting; formation of metal droplets; temperature distribution; electrode tip shape; numerical simulation

PACS: 44. 35.+C, 47. 27. E-, 47. 50. Cd, 47. 65. -d

1 Introduction

The electroslag remelting (ESR) process is a foundry method to refine and mold molten metals based on the electrical heating technique [1]. The Joule heating generated from the molten slag pool is used to melt the consumable electrode tip. The melting metal droplets at the tip of electrode go through the slag cover and come together in the molten metal pool. And finally they are solidified in the cooling water mold to form the high quality, low defects and segregation ingots [2]. Generally, the performance of ingot is characterized by its surface and internal performance, which depends intensively on the temperature and profile of melting pool [3]. The desired condition of the ESR process is a shallow metal melting pool which elevates unidirectional (upwards) solidification of the metal [4].

In order to improve the efficiency of ESR furnace and the ingot performance, the vibrating electrode electroslag remelting (VE-ESR) process has been proposed. Wang *et al.* [5] points out the vibrating electrode ESR technique would increase melting rating, improve heat transfer characteristic between electrode and slag, and even raise the temperature in slag layer. Figure 1 shows a schematic of the VE-ESR system.

In the ESR process, the electrode tip is supposed to effect the formation of metal droplets, while it will change the shape and size of metal droplets, further dominating the temperature profile in slag [6]. Because the change of the electrode tip dramatically influences the distribution of electrical currents in the slag, and so does the distribution of Joule heating. Furthermore, it has been concerned

***Corresponding Author: Fang Wang:** Key Laboratory for Ecological Metallurgy of Multimetallic Ores (Ministry of Education), Northeastern University, Shenyang, Liaoning Province 110819, China; School of Metallurgy, Northeastern University, Wenhua Road 3-11, Heping District, Shenyang, Liaoning Province 110819, China; Email: wangfang@smm.neu.edu.cn

Jakov Baleta: Faculty of Metallurgy, University of Zagreb, 44 103 Sisak, Croatia

Qiang Wang: Wuhan Univ Sci & Technol, State Key Lab Refractories & Met, Wuhan 430081, Hubei, China

Baokuan Li: School of Metallurgy, Northeastern University, Shenyang, 110819, China

that the metal pool shape plays an important role on the solute transport and macrosegregation in the ESR ingot [7]. Therefore, the effect of the electrode tip on the formation of metal droplets and temperature field should be systematically understood.

In the past, dedicated amount of work was done by choosing the flat tip electrode in the multi-physical fields. Jiang *et al.* [8] established a transient 2D axisymmetric numerical model with flat tip electrode to reveal the effect of metal droplets on the electromagnetic field, fluid flow and temperature field in the ESR process. Kharicha *et al.* [9] studied the influence of the frequency of AC power supply on the magneto-hydrodynamic with flat electrode tip during the traditional ESR process. The influence between the electrochemistry and the droplet formation is discussed. Kelkar *et al.* [10] studied the effect of the various process parameters on temperature profiles, flow field, and pool shapes with flat electrode tip in the traditional ESR process. Wang Q *et al.* [11] employed a transient 3D model to understand the role of slag thickness on the formation of metal bath with flat electrode tip in the ESR process. They found that changing the slag thickness could non-monotonically alter the slag temperature. However, they are all discussed about flat electrode tip during the traditional ESR process.

As discussed above, few attempts to systematically discuss the effect of electrode tip on the formation of metal droplets and temperature field in the vibrating electrode ESR furnace are found. In order to put the vibration electrode ESR system into practice, a further parametric study should be conducted. The aim of the present work is to study the effects of electrode tip profile on the formation of metal droplets and temperature field in the VE-ESR process. A transient full-coupled mathematical model with magneto-hydro-dynamic (MHD) multi-phase approach coupled with the dynamic mesh-based method has been established in the electromagnetic-controlled VE-ESR furnace. In addition, the effect of amplitude and frequency of electrode vibration have been discussed.

2 Mathematic Model

In the paper, the impact of electrode vibration on the electromagnetic field is neglected. The computational domain are composed of the slag and ingot.

The basic electromagnetic equations for the whole zone are as follows:

Ampere's la:

$$\nabla \times \vec{H} = \vec{J} + \frac{\partial \vec{D}}{\partial t} \tag{1}$$

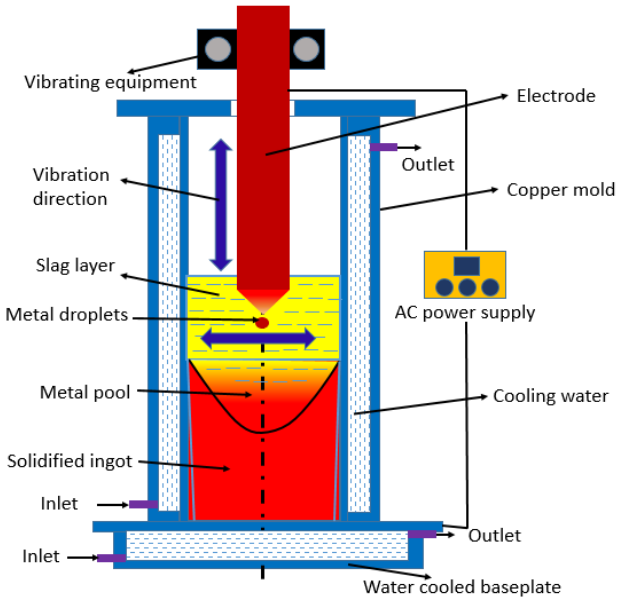

Figure 1: Schematic of the VE-ESR process; the purple arrows represent the direction of horizontal and vertical electrode vibration, respectively

Faraday's law:

$$\nabla \times \vec{E} = -\frac{\partial \vec{B}}{\partial t} \tag{2}$$

Gauss's law:

$$\nabla \cdot \vec{D} = \rho \tag{3}$$

Continuity of magnetic flux density:

$$\nabla \cdot \vec{B} = 0 \tag{4}$$

The displacement of electric current is much lower than electric conduction while the frequency is less than 50 Hz [12]. So that Ampere's law is simplified as: $\nabla \times \vec{H} = \vec{J}$

Ohm's law:

$$\vec{J} = \sigma(\vec{E} + \vec{v} \times \vec{B}) \tag{5}$$

Lorentz's law:

$$\vec{F} = \vec{J} \times \vec{B} \tag{6}$$

Joule's law: Fluid flow does not effect the magnetic field, as the magnetic Reynolds number keeps lower [13]. Thus, the Ohm's law has been simplified to $\vec{J} = \sigma\vec{E}$,

Joule heat generation rate is expressed as:

$$\vec{\omega} == \frac{Q}{t} = \frac{(J^2/\sigma)}{t} = \sigma\vec{E}^2 \tag{7}$$

The flow of the slag and liquid metal are supposed to be turbulent, as previously discussed by Jardy *et al.* [13]

and Kelkar *et al.* [14]. Hence, it is modeled based on Reynolds-averaged Navier-Stokes equations, through taking apart the local velocity into a mean and a fluctuation value. A standard k-ϵ turbulent model is employed to solve the turbulent viscosity of the momentum equations as follows:

$$\frac{\partial \rho}{\partial t} + \nabla \cdot \rho \vec{v} = 0 \tag{8}$$

$$\frac{\partial (\rho \vec{v})}{\partial t} + \rho(\vec{v} \cdot \nabla)\vec{v} = -\nabla \vec{P} + \nabla \cdot (\mu_{\text{eff}} \cdot \nabla \vec{v}) + \vec{F}$$

The volume of fluid (VOF) method presented in 'FLUENT' software are introduced since it is a robust, widely applied technique [5]. The user defined function (UDF) and dynamic mesh model are unified to performance the behavior of vibrating electrode.

$$\vec{F} = \vec{F}_e + \vec{F}_b + \vec{F}_p \tag{9}$$

Where, $\vec{F}_e$ and $\vec{F}_b$ + denotes the Lorentz force and buoyancy force, respectively. The buoyancy force is decided by the Boussinesq approximation [15]. The source term $\vec{F}_p$ is implemented to block the velocity to zero in the mushy zone.

The heat transfer and solidification feature in the ESR process are described by the energy conservation equation based on the enthalpy-formulation [16]:

$$\frac{\partial}{\partial t}(\rho H) + \nabla \cdot (\rho \vec{v} H) = \nabla \cdot (\lambda_t \nabla T) + Q_{Joule} \tag{10}$$

Where, λ_t denotes the effective thermal conductivity which is inferred from the turbulent viscosity [17], Q_{Joule} is Joule heating.

3 Boundary conditions and solution procedure

At inlet and outlet, the magnetic flux density is continuous and equal to zero near the wall [13] and $M_x = M_y = \frac{\partial M_z}{\partial z} = 0$; Wall: $M_x = M_y = 0$ and $M_z = \frac{I}{2\pi r}$. Evolution of the melting rate is solved by an iterative method, as follow [12]:

$$w = \frac{\psi Q_t}{V_{slag} \cdot L_{slag}} \tag{11}$$

Here, the symbol ψ represents the power efficiency. It is hard to decide the power efficiency accurately as to the complex physical and chemical process. Hence, a reasonable power efficiency 0.18 is chosen from literature [18].

A no-slip boundary condition is imposed at the mold walls. The top surface of slag are forced with zero shear stress. Inlet metal temperature profile was drawn with a parabolic shape, which had a 30 K superheat higher than the metal liquidus. Equivalent heat transfer coefficients are applied for the lateral and bottom walls [18, 19]. The key geometrical and material properties together with controlling parameters are shown in Table 1.

Table 1: The key geometrical, material properties and controlling parameters used in simulation

Parameter	Value
Geometry and operating conditions	
Electrode diameter (m)	0.1
Slag bath depth (m)	0.12
Immersion depth of electrode (m)	0.1
Ingot diameter (m)	0.22
Current (A)	4500
Frequency (Hz)	50
Vibrating amplitude, m	0.003
Vibrating Frequency, c/min	20
Interfacial tension between slag and metal, N/m	0.9
Physical properties of metal	
Density ($kg{\cdot}m^{-3}$)	7800
Viscosity ($kg{\cdot}m^{-1}{\cdot}s^{-1}$)	0.0061
Specific heat ($J{\cdot}kg^{-1}{\cdot}K^{-1}$)	866
Thermal conductivity ($W{\cdot}m^{-1}{\cdot}K^{-1}$)	35
Electrical conductivity ($\Omega^{-1}{\cdot}m^{-1}$)	$7.14{\times}10^5$
Latent heat of solidification ($J{\cdot}kg^{-1}$)	$2.77{\times}10^5$
Liquidus temperature (°C)	1784
Solidus temperature (°C)	1716
Physical properties of slag	
Density ($kg{\cdot}m^{-3}$)	2800
Viscosity ($kg{\cdot}m^{-1}{\cdot}s^{-1}$)	0.3
Specific heat ($J{\cdot}kg^{-1}{\cdot}K^{-1}$)	1255
Thermal conductivity ($W{\cdot}m^{-1}{\cdot}K^{-1}$)	10.46
Electrical conductivity ($\Omega^{-1}{\cdot}m^{-1}$)	$\ln\sigma = -6769.0/T + 8.818$
Liquidus temperature (°C)	1650
Top surface emissivity	0.6

The commercial software FLUENT is used to simulate the VE-ESR process ground on the finite volume method. While the electromagnetic field computed by the MHD module is not proper for the ESR furnace, we programed and developed the MHD module with user-defined functions based on the Maxwell equations. Controlling equations including electromagnetic phenomenon, fluid flow, heat transfer and metal pool profile are iteratively solved. The motion of vibrating electrode is traced by a dynamic mesh-based approach. The second order upwind is used

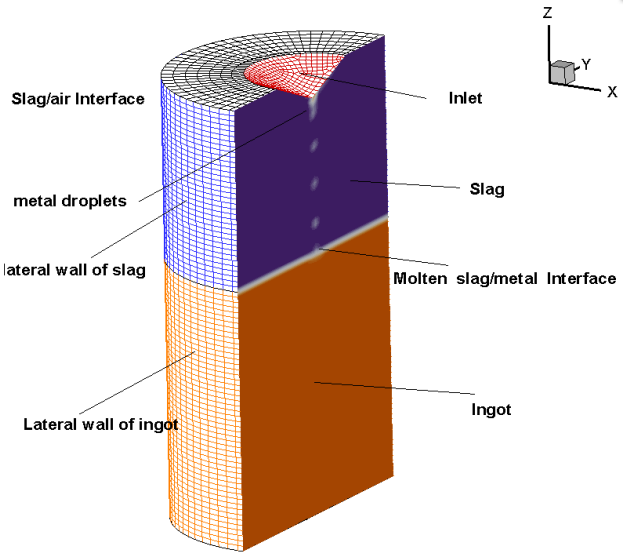

Figure 2: Structure mesh used in the present work

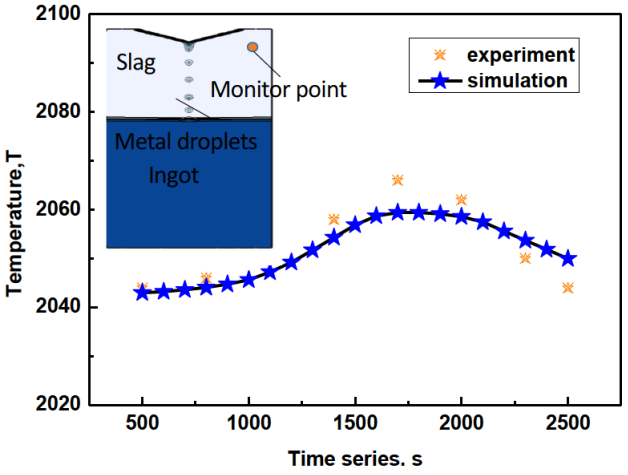

Figure 3: Time series of temperature between experiment and simulation

to discretize all the equations. The iterative procedure will not stop until the normalized residuals is below 10^{-6}. The computational zone is gridded with the structured mesh. In order to insure the reasonability of convergence criteria, the time step is set to be 0.001s. It takes about 160 CPU hours in parallel mode (HPC of 8 cores and 3.10 GHz) to obtain a convergent result. In order to check out the dependence of mesh, the three meshes of 124,000, 245,000, and 402,000 control volumes are performed, respectively. Due to the longer computational time, the middle mesh is used, shown in Figure 2.

4 Model validation

In order to verify the reliability of mathematical model, the temperature between the plant experiment and numerical simulation has been compared. The plant-scale experiment with a vibration electrode on an ESR furnace has been conducted in Shenyang Research Institute of Foundry. The inner diameter, height, and wall thickness of mold were 220×1000×71 mm. The 4500 A and 50 Hz current was used. The cylindrical electrode was made of Q235 carbon steel, approximately 110mm in diameter. The normal slag composition was 70%wt of calcium fluoride and 30%wt of aluminum oxide. The slag cover thickness was maintained at 120 mm during the whole process. The monitor points of slag temperature is measured by a disposable W3Re/W25Re thermocouple. The vibrating electrode containing the laser amplitude sensor was laid out and manufactured following the classic vibration technology. The experimental conditions are as the same as the simulation. Five groups of experiment results are obtained and the averaged value are used. Figure 3 represents the time series of temperature between experiment and simulation. The position of measurement is defined at monitor point as it is convenient for us to arrange the thermocouple during the experiment. The calculation results are in accord with experimental results, hence it is indicated that the mathematical models used in this work are reliable and effective.

5 Results and Discussions

Figure 4 presents formation of metal droplets and electromagnetic force distribution under horizontal vibration with flat tip electrode during the whole period (3s). The high electrical resistance of slag provides plenty of energy to melt the electrode tip, leading to the formation of metal droplets. It can be found that the horizontal motion of electrode is transferred to the metal droplets horizontal velocity. The metal droplets flow periodically downward and during this process, they are prone to concentrate in the center of electrode tip, so they become larger and stretched. This is not beneficial to the inclusion removal. The metal droplets in the slag have higher electrical conductance, so the maximum current is located nearby the metal droplets. Hence, the electromagnetic force is distributed intensively around them. Joule heating is determined by the current and electrical resistance of the slag. As the slag resistance is considered constant, the distribution of Joule heating is similar to that of current density.

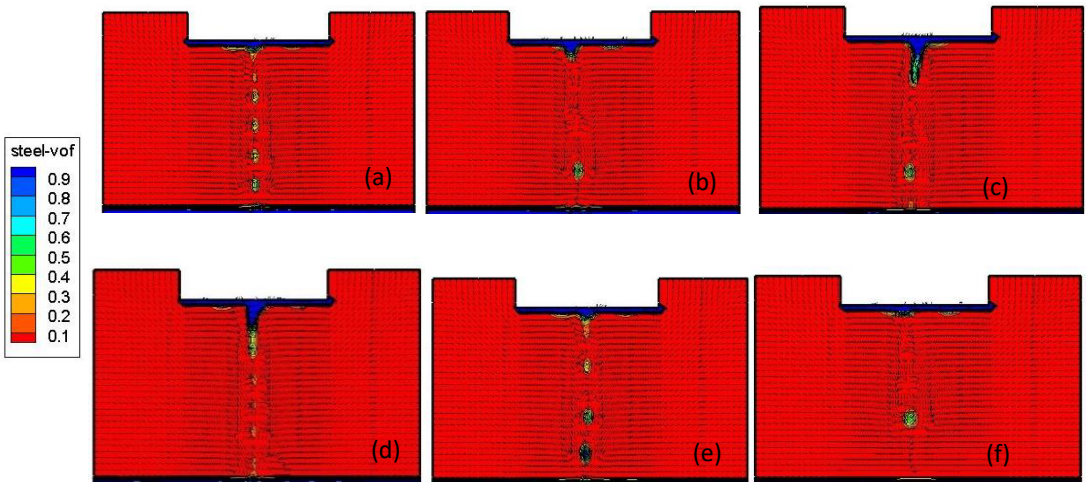

Figure 4: Formation of metal droplets and electromagnetic force distribution under horizontal vibration with flat tip electrode (a) T=0s (b) T=0.5s (c) T=1s (d) T=1.5s (e) T=2.0s (f) T=2.5s

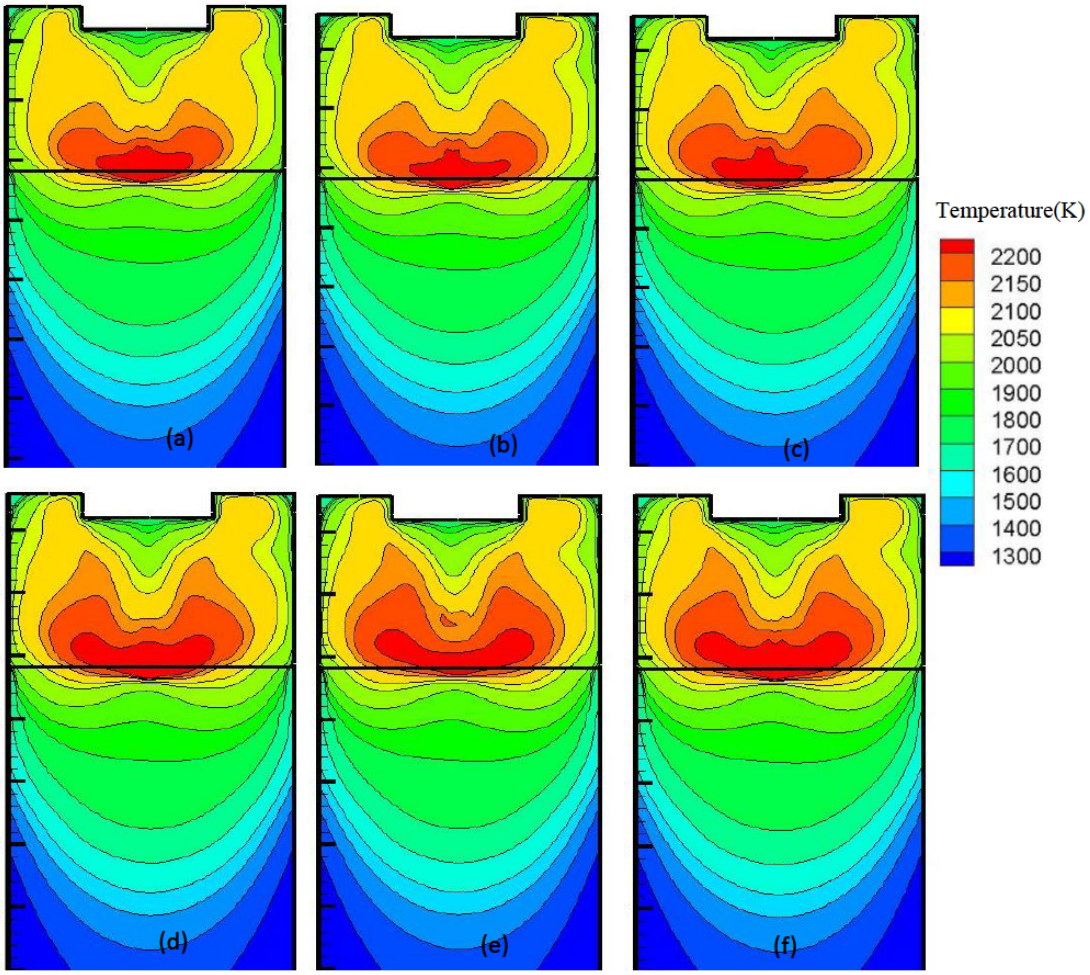

Figure 5: The distribution of temperature under horizontal vibration with flat tip electrode (a) T=0s (b)T=0.5s (c) T=1s (d) T=1.5s (e) T=2.0s (f) T=2.5s

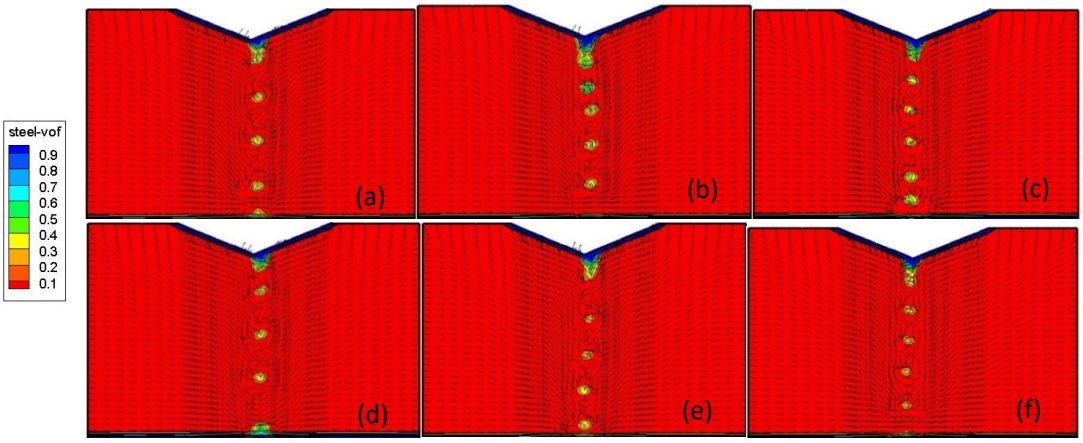

Figure 6: The distribution of droplets and electromagnetic force under horizontal vibration with cone tip electrode (a) T=0s (b) T=0.5s (c) T=1s (d) T=1.5s (e) T=2.0s (f) T=2.5s

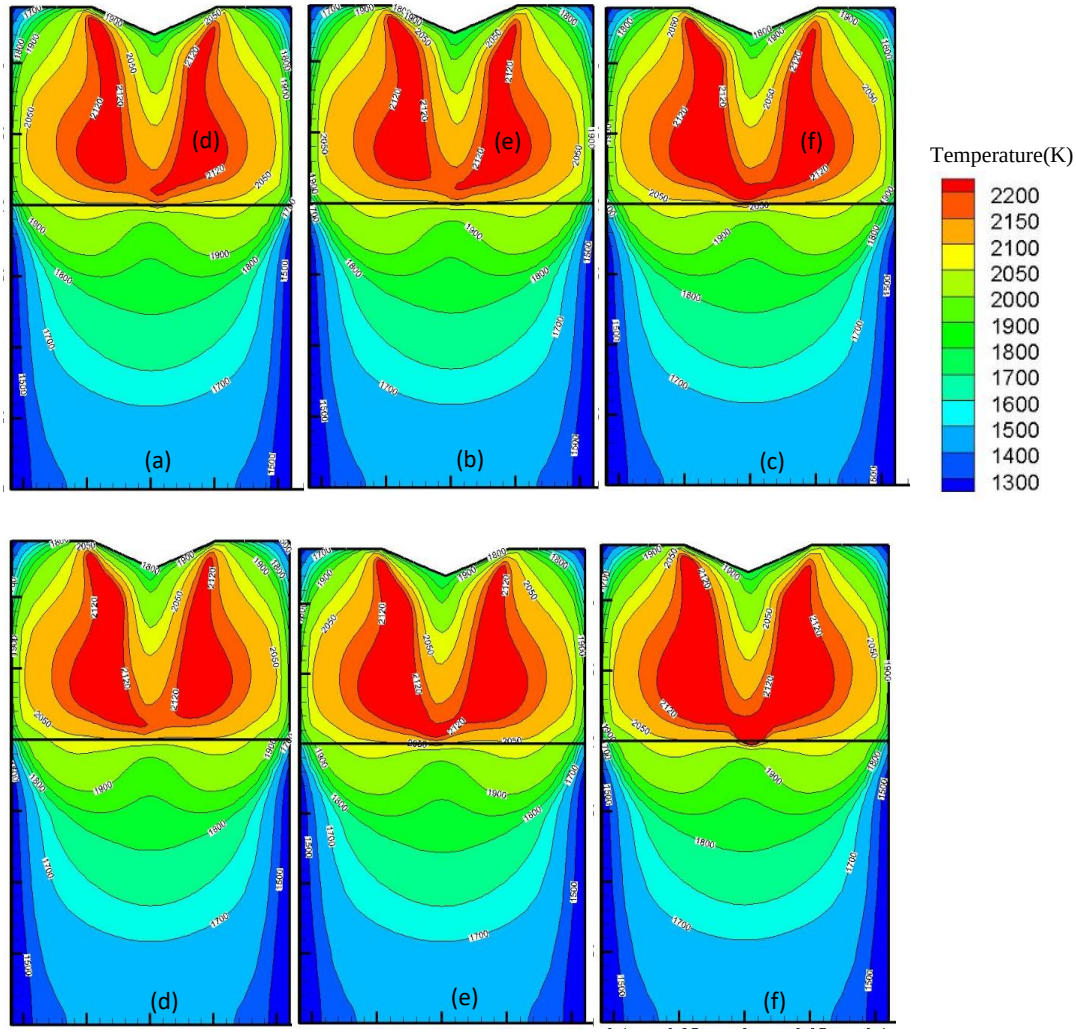

Figure 7: The distribution of temperature under horizontal vibration with cone tip electrode in a whole period (3s) (a) T=0s (b) T=0.5s (c) T=1s (d) T=1.5s (e) T=2.0s (f) T=2.5s

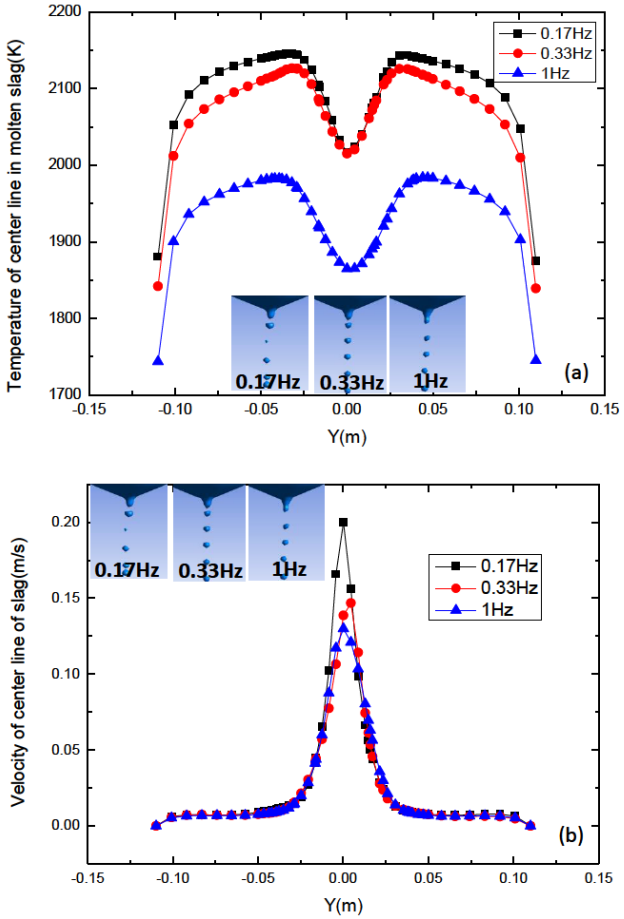

Figure 8: (a) temperature distribution and (b) velocity distribution of the center of molten slag under horizontal vibration with different frequency at 2100s

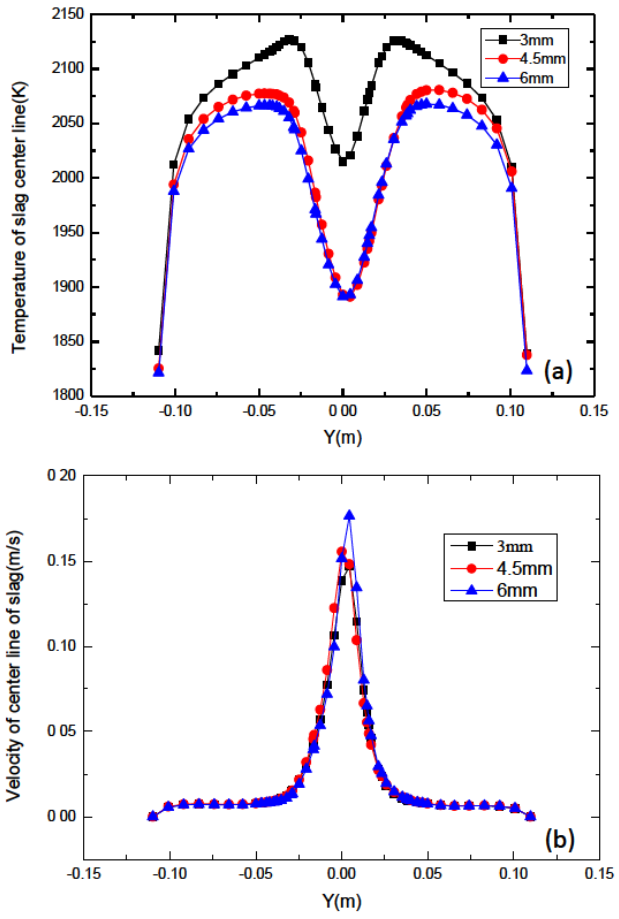

Figure 9: (a) temperature distribution and (b) velocity distribution in the center line of molten slag under horizontal vibration with different amplitude at 2100s

The distribution of temperature under horizontal vibration with flat tip electrode is shown in Figure 5. While the temperature field is related to the Joule heating and boundary conditions, it is also influenced by the dripping metal droplets and fluid flow of molten slag and metal during VE-ESR process. The maximum temperature occurs in the lower slag layer. Its location will vary periodically over time, depending on the vibration frequency and amplitude.

The distribution of droplets and electromagnetic force under horizontal vibration with cone tip electrode are depicted in Figure 6. The same tendency can be observed as in the case with the flat tip electrode. The metal droplets have the uniform periodical behavior and the horizontal velocity. However, the average dimension of the metal droplets is smaller. In addition, larger and stretched metal droplets are not observed. The reason for that behavior lies in the fact that the cone tip electrode accelerates metal droplets towards the center by the gravity force. In the meantime, the horizontal velocity makes them easily separated from the electrode tip. The distributions of temperature under horizontal vibration with cone tip electrode during one period (3s) are shown in Figure 7. Contrary to the flat tip electrode case, temperature fields are periodically distributed, aligned with electrode motion. The maximum temperature zone is located along the slag depth, not in the lower part.

The temperature and velocity distributions in the center line of molten slag under horizontal vibration with different frequency are demonstrated in Figure 8. It can be seen that with the increase in vibration frequency, the maximum temperature decreases. When the frequency changes from 0.17Hz to 1Hz, the maximum temperature reduces from 2050K to 1985K because vibrations can accelerate heat transfer between the slag and mold. Velocity distribution is different from the temperature field; the maximum is located in the center and the minimum at the wall. The metal droplets falling down through the slag

layer have larger velocity. Since the electrode vibrates in the horizontal direction, the peak along the center line deviates. When the frequency id increased, the peak value of velocity is decreased from 0.20m/s to 0.125 m/s. Since the metal droplets become smaller, the dripping velocity dominated by the gravity force decreases.

The temperature distributions and velocity distributions in the center line of molten slag under horizontal vibration with different amplitudes are represented in Figure 9. From the picture, it could be seen that with the increase in vibration amplitude, the maximum temperature in the slag drops. When the vibration amplitude varies from 3mm to 6mm, temperature decreases by 3.9%. The velocity tendency is similar to the case in Figure 8(b). When the vibration amplitude changes from 3 mm to 6 mm, the peak value of velocity rises by 16.7%, from 0.15m/s to 0.175m/s, because electrode vibrations force the flow of nearby molten slag.

6 Conclusions

A transient full-coupled mathematical model with magneto-hydro-dynamic (MHD) multi-phase approach coupled with a dynamic mesh-based method has been established in the electromagnetic-controlled VE-ESR furnace. The effect of tip profile of electrode on formation of metal droplets and temperature field has been analyzed in the VE-ESR process. The effect of amplitude and frequency of electrode vibration on velocity and temperature field have been discussed.

In the case of the cone tip electrode, the average dimension of metal droplets is smaller compared to the flat tip electrode. In addition, larger and stretched metal droplets are not observed in the case of the cone tip electrode. The temperature field in the cone tip electrode case is distributed periodically, contrary to the flat tip electrode. The maximum temperature zone with the cone tip electrode is located along the z axial in the upper part of slag, not in the lower part. When the frequency changes from 0.17 Hz to 1 Hz, the maximum temperature reduces from 2050K to 1985K and the peak value of velocity decreases from 0.20 m/s to 0.125 m/s. When the vibration amplitude varies from 3 mm to 6 mm, the maximum temperature in the slag cover drops by 3.9% and the peak value of velocity rises by 16.7%.

Acknowledgement: The authors acknowledge Key Program of Joint Funds of the National Natural Science Foundation of China and the Government of Liaoning Province (Grant No.U1508214).

References

[1] Kharicha A., Karimi-Sibaki E., Wu M., Ludwig A., and Bohacek J., Review on Modeling and Simulation of Electroslag Remelting, Steel Res. Int., 2018, 89(1), 1700100.

[2] Dub V.S., Levkov L.Ya., Shurygin D.A., Tolstykh D.S. Klochai V. V. Korzun E. L. Garchenko A. A., Electroslag remelting technology for contemporary engineering, retrospection and new possibilities, Metallurgist, 2018, 62(5-6), 511-520.

[3] Detrois M., Jablonski P.D., Hawk, J.A., Evolution of tantalum content during vacuum induction melting and electroslag remelting of a novel martensitic steel, Metall. Mater. Trans. B., 2019, 50(4), 1686-1695.

[4] Baligidad R.G., Prakash U., Rao V.R., Rao P.K., Ballal N.B., Development of Fe3Al based intermetallic alloys by electroslag remelting, ISIJ Int., 1995, 35(4), 443-445.

[5] Wang F., Lou Y.C., Chen R ., Song Z.W., Li B.K., Effect of vibrating electrode on temperature profiles, fluid flow, and pool shape in ESR system based on a comprehensive coupled model, China Foundry, 2015, 12(4), 285-292.

[6] Kharicha A., Wu M., Ludwig A., Simulation of the electric signal during the formation and departure of droplets in the electroslag remelting process, Metall. Mater. Trans. B. 2016, 47, 1427-1434.

[7] Fezi K., Yanke J., Krane M.J.M., Macrosegregation during eectroslag remelting of alloy 625, Metall. Mater. Trans. B. 2015, 46(2), 766-779.

[8] Yu J., Jiang Z., Liu F., Chen K., Li H., Geng X., Effects of metal droplets on electromagnetic field, fluid flow and temperature field in electroslag remelting process, ISIJ Int., 2017,57 (7), 1205-1212.

[9] Kharicha A., Wu M., Ludwig A., Ramprecht M., Holzgruber H., Influence of frequency of the applied ac current on the electroslag remelting process, Symposium on CFD Modeling and Simulation in Materials Processing held during the TMS Annual Meeting and Exhibition, 2012, 139-146.

[10] Kelkar K.M., Patanker S.V., Mitchell A., Computational model of the Electroslag remelting (ESR) process used for the production of ingots of high-performance alloys, Proceedings of the 2005 International Symposium on Liquid Metal Processing and Casting, 2005, 137-144.

[11] Wang Q., Liu Y., Wang F., Li B., Numerical study on the effect of electrode polarity on desulfurization in direct current electroslag remelting process, Metall. Mater. Trans. B.,2017, 48(5): 2649-2663.

[12] Weber V., Jardy A., Dussoubs A., A comprehensive model of the electroslag remelting process: description and validation metal, Mater. Trans. B 2009, 40(3), 271-280.

[13] Jardy A., Ablitzer D., Wadier J. F., Magnetohydrodynamic and thermal behavior of electroslag remelting slags, Metallurgical transactions. B, 1991, 22(1):111-120.

[14] Kelkar K.M., Patankar S.V., Mitchell A., Computational modeling of electroslag remelting processes, Journal de Physique IV (Proceedings), 2004, 120:421-428.

[15] Wang Q., Wang R., He Z., Li G., Li B., Li H., Numerical analysis of inclusion motion behavior in electroslag remelting process, Int. J. Heat Mass Transfer., 2018, 125, 1333-1344.
[16] Plotkowski A., Krane M.J.M., The use of inverse heat conduction models for estimation of transient surface heatflux in electroslag remelting, J. Heat Transfer, 2015, 137(3), 031301.
[17] Dong Y., Hou Z., Jiang Z, Liu H., Study of a single-power two-circuit ESR process with current-carrying mold: mathematical simulation of the process and experimental verification, Metall. Mater. Trans. B., 2018, 49(1), 349-360.
[18] Wang F., Wang Q., Li B.K., Comparison of Thermo-electromagneto-hydrodynamic Multiphysical Fields in ESR Furnace with Vibrating and Traditional Electrodes, ISIJ Int. 2017, 57(1) 91-99.
[19] Wang F., Xiong Y., Li B., Impact of Fill Ratio on Temperature Profile and Metal Bath Configuration in Electroslag Remelting Process With Vibrating Electrode, Steel Res. Int., 2019, 90(4), 1800092.